Tellus **000**, 000–000 (0000) Printed 2 May 2005 (Tellus LaTeX style file v2.2)

A new climatology of reverse-shear polar lows

By ERIK W. KOLSTAD[1]*
[1] *Bjerknes Centre for Climate Research, Allégaten 70, 5007 Bergen, Norway*

(N/A)

ABSTRACT

A new climatology of reverse-shear polar low development is presented. In reverse-shear flow, the wind at the low-level steering level is in the opposite direction of the thermal wind in the adjoining layers. A framework for identifying such conditions along with weak lower-level static stability from any gridded data is developed by defining simple dynamical constraints on standard atmospheric fields, applied here to 40 years of 6-hourly coarse-resolution ERA-40 data. There are several areas where such conditions occur with high frequency: the Norwegian Sea (> 15 % of the time during NDJFM), the region to the south of the Denmark Strait (> 10 %) and the Bering Sea and the Sea of Okhotsk (> 5 %). The latter regions follow a distinct seasonal cycle, with a maximum of activity towards new-year. In the Nordic Seas region, the polar low season is longer because the air temperature stays low throughout March. There are primary peaks in December and January and a secondary peak in March, preceded by a distinct nadir in February. This is due to the high (low) frequency of reverse-shear conditions in March (February), because of the sharp increase in the NAO index from its yearly minimum in February to March.

1 Introduction

Polar lows are intense mesoscale low-pressure systems, usually generated by outbreaks of cold, dry polar air over warm water masses. There is a range of conditions leading to such developments, sometimes referred to as the 'polar low spectrum' (Rasmussen and Turner, 2003). An important group of polar lows are the reverse-shear systems. With these, the conditions are such that the wind at the low-level steering level is antiparallel to the thermal wind in the adjoining layers (Duncan, 1978). The wind speed generally decreases with height and there is a forward tilt of the disturbances in the vertical direction (Rasmussen and Turner, 2003). Large ocean-air heat fluxes in cold air masses may lead to release of latent heat, further intensifying the development (e.g. Montgomery and Farrell, 1992). Typical examples of such conditions occurs in positive phases of the North Atlantic Oscillation (NAO), when warm synoptic-scale storms enter the Norwegian Sea from the south (e.g Rogers, 1997). If the cold fronts of such systems are connected to the inversion over the ice, dry polar air will be pulled southwards, lowering the static stability in the region (e.g. Wu et al., 2004). This has a significant effect on the mesoscale development in the area (Harold et al., 1999).

While reverse-shear conditions are generally considered to be important for polar lows to develop, few attempts have been made to quantify how often these conditions occur, and how often they lead to polar low development. It is therefore attempted here to quantify how often, as well as when and where such systems are likely to develop. Due to their small spatial and temporal scales, polar lows are difficult to track objectively. Because of this, certain simple dynamical constraints are defined here to identify 'favourable' synoptic conditions for reverse-shear polar low development in the ERA-40 reanalysis data set. The behaviour of these constraints will be validated against a selection of reverse-shear polar lows which have been investigated in other studies.

The main objectives of this study are: 1) to quantify the climatological distribution of such conditions in the current climate, and 2) to provide a framework for identifying such conditions in any data set, e.g. in simulations of future climate scenarios. Accordingly, only basic atmospheric fields at standard pressure level surfaces are used in the analysis.

2 Reverse-shear polar lows

Duncan (1977) found that the existence of a vertical wind shear and that the thermal wind and steering-level winds were parallel were necessary conditions for polar lows to develop. Later, he showed that reverse-shear conditions could also be favourable (Duncan, 1978). He used atmospheric conditions in the region of a recorded polar low in a simulation, and found that the most unstable wave in his model had a wavelength of 900 km, resembling the observed system.

Wilhelmsen (1985) studied synoptic weather charts spanning a period of 11 years (1972-82) and found 32 polar lows in the Norwegian and Barents Seas. The propagation of these being mostly from the north, the majority of them were most likely embedded in reverse-shear flow. The Norwegian Atlantic Current brings warm, saline water into

* Corresponding author.
e-mail: erik.kolstad@bjerknes.uib.no

this region (Orvik and Niiler, 2002), leading to high sea surface temperatures at high latitudes even in mid-winter (Rasmussen and Turner, 2003). In positive phases of the NAO, storms tend to extend into the Norwegian and Barents Seas from the south-west. The proximity of the Arctic ice sheet then frequently leads to low static stability and reverse shear in the northerly flow following the cold fronts of such lows. Harold et al. (1999) found that mesocyclones in the 200-400 and 400-600 km size range were significantly correlated with the NAO index. As the index became more positive, the small to midsized mesocyclones were more likely to develop. Furthermore, it was noted that such mesocyclones often develop behind synoptic-scale cyclones. For the reasons stated above, the Norwegian and Barents Seas region is considered the primary region for polar lows (Rasmussen and Turner, 2003), and numerous observational and numerical studies of reverse-shear systems have been focussed in this area.

Grønås et al. (1987) used a limited area model to simulate polar lows in the Norwegian Sea, all of them in reverse-shear conditions in northerly flow. The structures were found to be shallow (mainly below 700 hPa) and it was suggested that CISK-like mechanisms intensified the developments.

Four reverse-shear polar lows over the Greenland Sea were studied by Reed and Duncan (1987). The model used by Duncan (1977) was used and the fastest growing modes had wavelengths in the 300-1000 km range. The disturbances created by their model were mostly confined to the atmosphere below 700 hPa.

Grønås and Kvamstø (1995) investigated four cases with reverse-shear synoptic conditions favourable for polar lows and found that the height between the tropopause and the convective planetary boundary layer gave a good indication of the possibility for polar low development. In only two of their cases actual polar lows formed, and then that height was 1000 m or less. It was also claimed that northerly winds from an inversion over the ice is a necessary condition for polar low development. Other studies of polar lows in the Nordic Seas region (Nordeng and Rasmussen, 1992; Rasmussen et al., 1992; Claud et al., 2004) will be used to validate the criteria for 'favourable conditions' defined below.

Bond and Shapiro (1991) examined two polar lows in reverse shear over the Gulf of Alaska. Baroclinic instability and release of latent heat was found to represent the main source of eddy kinetic energy in these cases. Mailhot et al. (1996) studied a polar low over the Labrador Sea with strong surface winds and strong low-level baroclinicity in reverse shear. In two studies of a polar low over the Japan Sea (Yanase et al., 2002; Fu et al., 2004), reverse shear is never mentioned explicitly, but it will be seen below that this development took place in such conditions. The two latter developments are also used below to validate the criteria.

3 Definition of criteria

Polar lows are usually confined to the lower levels of the troposphere, so the typical steering level is taken to be at either 775 or 850 hPa. This is consistent with steering-level winds used in simulations based on observational records (eg. Duncan 1978). Following Holton (2004), the wind direction at these levels is compared to the direction of the thermal wind in the 700-925 hPa layer, calculated as

$$u_T = -\frac{1}{f}\frac{\Delta(\phi_{700} - \phi_{925})}{\Delta y}, \qquad v_T = \frac{1}{f}\frac{\Delta(\phi_{700} - \phi_{925})}{\Delta x}.$$

The angle α_S between these winds is then given by

$$\cos\alpha_S = \frac{\mathbf{v}_T \cdot \mathbf{v}_S}{|\mathbf{v}_T||\mathbf{v}_S|},$$

where $\mathbf{v}_S$ is the wind at either 775 or 850 hPa. The first criterion for 'favourable conditions' used here is that at least one of these angles is close to 180°, corresponding to a reverse thermal shear with respect to one of the two possible steering levels. From a qualitative examination of cloud structures in satellite images, it seems that an angle of no more than 45° from the antiparallel between the thermal wind and the wind at the steering level is sufficient to favour baroclinic development.

As well as reverse thermal shear, low static stability in the lower atmosphere and advection of cyclonic vorticity aloft are considered crucial for polar lows to develop (e.g. Rasmussen and Turner, 2003). It is known from considerations of potential vorticity and thermal wind balance that these two features are closely correlated (Bluestein, 1993). With this relationship in mind, one can consider the stability in the lower levels, e.g. up to the 700-hPa surface, a tracer of upper-level disturbances. The Rossby radius of deformation is defined in Holton (2004) as

$$L_R \equiv NH/f_0,$$

where f_0 is the Coriolis parameter, H is the height of the tropopause and N is the Brunt-Väisällä frequency. Small values of N allow upper-level disturbances to penetrate greater vertical distances and even small-scale disturbances aloft are able to reach far down towards the surface. To quantify the lower-level static stability, a dimensionless normalized radius of deformation defined as

$$R_N \equiv L_R/H = N/f_0$$

is used. N is calculated in the 700-925 hPa layer as the real part of

$$N = \sqrt{g\frac{\Delta(\ln\theta)}{\Delta z}}.$$

The second criterion for favourable polar low conditions is that R_N must be small. Using one discrete boundary is somewhat arbitrary. However, deciding against splitting the analysis in two or more parts, using different thresholds for R_N, 25 is taken as the upper boundary. This is based on an empirical trial and error procedure, using satellite images as a qualitative reference.

Six-hourly atmospheric data from the ERA-40 gridded reanalysis project for the polar low season from October to April from 1960-61 to 1999-2000 are used in the analysis. The horizontal resolution of the data is 2.5° by 2.5°, corresponding to a distance of 280 km in the zonal direction between the grid points at the equator and half of that at 60°N. The coarse-resolution version of the ERA-40 data was chosen instead of the one with higher horizontal resolution (1.125° by 1.125°), because the latter version includes mesoscale features. Since the intent here is to look at synoptic 'background' conditions, this would introduce noise in

the data. For each 6-hourly values, the parameters are calculated for each grid point from 40°N and northwards. When both the criteria, i.e. $135^\circ \leqslant \alpha_S \leqslant 225^\circ$ and $R_N \leqslant 25$, are fulfilled, the location and time of the polar low *potential* are recorded. To quantify the seasonal cycle inside selected regions, the percentage of the total number of grid points with such potential in each region was calculated.

An approach such as this, using rigid thresholds as constraints on atmospheric fields, only gives a qualitative measure of the probability of polar low development. Nevertheless, it will be seen in the following section that the criteria correspond quite well with actual polar lows.

4 Validation of criteria

The above selection of constraints was based on previous studies of the mechanisms leading to reverse-shear polar low development. Here, satellite images are compared to maps of potential polar lows.

4.1 14-15 October 1993; Norwegian Sea

This polar low development has been studied in great detail in Claud et al. (2004), where it was dubbed 'le Cygne' due to its swan-like appearance. With a lifetime of roughly 72 hours, this was an unusually long-lived polar low. Inbetween a synoptic low (the cloud system seen at 72-73°N, 35°E in figure 1 in Claud et al., 2004) passing over Scandinavia from the south-west and a high over Greenland, a large portion of the Norwegian and Barents Seas was characterized by reverse shear and weak static stability in the lower layers. Inside this region, 'le Cygne' formed early on 14 October and moved in a southerly direction until its collapse in the North Sea on 16 October. A satellite image taken at 0525 UCT on 15 October 1993 is included here in figure 1. Figure 2 is a map illustrating the behaviour of the constraints at approximately the same time. The region with reverse shear is clearly seen inside the thick contour lines. This corresponds well with the convective cloud systems in the satellite image. Where this region coincides with the region of weak static stability (dashed contour line), there is potential for polar lows to develop (shaded). 'Le Cygne' is clearly inside this region. Moreover, inside the shaded region south of Svalbard, a polar low developed shortly after.

4.2 11-12 January 1989; Labrador Sea

This polar low in the Labrador Sea is studied in depth in Mailhot et al. (1996). In figure 3, a satellite image taken at 1509 UTC 11 January 1989, the polar low is clearly seen on the left. At this time, there is a synoptic-scale low situated to the south-west of Iceland, leading to the northerly winds in reverse-shear flow in the Labrador Sea. Figure 4 is a snapshot of the criteria at 0000 UTC on the 12th. The regions with reverse shear in the Labrador Sea are recognized from the cloud structures in the satellite image. The shaded region coincides quite well with the observed polar low.

4.3 21 January 1997; Japan Sea

A polar low observed in the Japan Sea on 21 January 1997 was investigated by Yanase et al. (2002) and Fu et al. (2004). It formed to the west of Hokkaido island and moved southeastward with a speed of about 40 km/h. Figure 5 is an image of the cloud-top equivalent blackbody temperature (TBB) estimated from Geostationary Meteorological Satellite-5 infrared data of the Japan Meteorological Agency, taken at 1800 UTC on that day. It is clearly seen that the flow in the area north of the development is from the north or north-east (as mentioned in Fu et al., 2004). No specific mention of reverse shear is made in either paper, but it can be seen from figure 6, a representation of the criteria at the same time, that almost the entire area displayed there has reverse shear. In the shaded area, there is low stability as well, and this area matches the cloud structures in figure 5.

4.4 26-27 February 1987; Barents Sea

This polar low was studied by by Nordeng and Rasmussen (1992). Figure 7 is a satellite image taken at 0418 UTC on 27 February 1987. On the synoptic scale, it is seen from the cloud streets to the north of the polar low that there is a large-scale low to its east, which cloud system can be seen in the image. The passage of this low across the Norwegian Sea led to a northerly flow, reverse shear and weak static stability in a large region. It can be seen from figure 8, an outline of the criteria at 0000 UTC on the same day, that the horizontal scale of the resulting polar low is quite large with the upper boundary of R_N in mind. If this specific boundary had been increased somewhat, the shaded area would have corresponded better with the cloud structures in the satellite image. Nevertheless, the development is clearly registered.

4.5 15 December 1982; Barents and Norwegian Seas

These multiple polar low developments have been studied in a number of papers summarized in Rasmussen and Turner (2003) (e.g. Rasmussen et al., 1992 and Grønås et al., 1987). Following a series of polar low developments in the Barents Sea in the days before 15 December, all of which are discussed in Rasmussen et al. (1992), almost the entire Norwegian Sea and parts of the Barents Sea had reverse shear. In addition, as seen in figure 10, the static stability is weak in the entire region. This leads to polar low potential in large portions of the area displayed. In a satellite image (figure 9) taken at 0406 UTC on the 15th, it is apparent that there is a lot of mesoscale activity in the region. The small-scale polar low dubbed 'L2' in Rasmussen and Turner (2003) and 'C' in (Rasmussen et al., 1992; their figure 13), is not picked out directly by the criteria. Due to the southerly winds associated with the cyclonic activity in the region at the time, the region to the immediate south-east of that activity did not have reverse shear at the time.

5 Climatology of reverse-shear polar lows

It has now been established that the criteria defined above identify favourable conditions for reverse-shear polar

low development. To investigate the climatology of those conditions, the number of cases over 40 seasons with polar low potential are counted.

5.1 Spatial distribution

In figure 11, the percentage of the time for each grid point during November to March (NDJFM) from 1960-61 to 1999-2000 with polar low potential is displayed. This map is similar to the spatial distribution of 200-400 km wintertime mesocyclones in Harold et al. (1999, their figure 2b). However, their maxima in the Denmark Strait and in the Norwegian Sea are both on the order of 2-3 percent (DJF occupation time). Recalling that the criteria used in this study do not select actual polar lows, this difference in magnitude is perhaps not so surprising. As expected, there is a distinct maximum of potentials in the Norwegian Sea, reaching into the Barents Sea. The constraints are satisfied roughly 10-15 percent of the time in that area. The region to the west and south-west of Iceland represents another local 'hot-spot' of such conditions. In the North Pacific, the Sea of Okhotsk and the Bering Sea are also quite frequently subject to such conditions. All in all, the maxima identified by the constraints agree quite well with other climatological results (Rasmussen and Turner, 2003).

In terms of reverse thermal shear, figure 12 shows the percentage of the total NDJFM period when $135^\circ \leqslant \alpha_S \leqslant 225^\circ$. In the North Atlantic, the most affected regions are those to the west and north-west of the mid-latitude storm tracks, with the warm air to the east, corresponding to a southerly thermal wind. The persistence of the reverse shear in the Denmark Strait is due to this region being 'trapped' between the Icelandic low and the Greenland High. However, the Greenland, Norwegian and Barents Seas regions are also prone to such conditions. This can also be said about the Bering Sea and the Sea of Okhotsk. On the whole, it is clear that the regions known for polar low development all have high frequencies of reverse shear.

The percentage of the wintertime when $R_N \leqslant 25$ is shown in Figure 13. The stability is generally quite weak in the Norwegian and Barents Seas, where the constraint on R_N is satisfied nearly half the time. The proximity of the ice edge and the large extent of relatively warm open water at high latitudes, combined with a high frequency of northerly winds following the passage of extratropical storms, are the main reasons for this. With the threshold value decreased to $R_N \leqslant 20$, the Norwegian Sea maximum is reduced to roughly 15 percent of the time (not shown). This parameter is, in other words, quite sensitive to small changes in R_N.

5.2 Seasonal cycle

With regards to the local maxima in figure 11, two regions were chosen for further analysis: a sector of the Norwegian Sea (NS from now on: latitudes from 67.5 to 75 and longitudes from -12.5 to 12.5) and a sector of the Sea of Okhotsk (SO: latitudes from 47.5 to 57.5 and longitudes from 145 to 155). The average percentage (over 40 seasons) of their respective total number of grid points with potential for polar lows every six hours from 1 October to 30 April is then calculated. As a consequence of the noisy nature of the resulting 'time series', daily means and simple second-order polynomial trends are displayed in figure 14. As expected, the winter is the most active polar low season. In all the regions, the peak of such activity occurs around new-year. In terms of daily means, the local peak in late March in the Norwegian Sea sector stands out. It is obvious that this peak is significant. Similarly, there is a nadir in mid- to late February. This is not altogether surprising, since the polar low activity is known to be relatively weak in February in the Norwegian Sea (Sigbjørn Grønås, personal communication).

The temporal distribution of reverse-shear conditions is displayed in figure 15. A peak is found near the end of March in the NS region, corresponding very well with the similar peak in figure 14. This strongly suggests that this peak is closely tied to storms passing through the region from the south-west, as these storms are instrumental in generating reverse-shear conditions in this region. As mentioned above, Harold et al. (1999) found the correlation between positive phases of the NAO and small to midsized mesocyclone activity in the Nordic Seas to be significant. The average monthly NAO index from May 1960 to April 2000 is displayed in figure 16. It is clear that according to the index, February generally represents a minimum of corresponding synoptic activity, thereby most likely decreasing the number of reverse-shear situations in the Norwegian Sea. It is also noted that there is a sharp increase in the index from February to March, complying with the peaks and nadirs in figures 14 and 15. However, there is not a one-to-one correspondence between the NAO index and reverse shear. For example, even though the index takes relatively high values in October, there is not an especially high frequency of reverse shear then in the Norwegian Sea compared to in March. This is because the air is much colder in March due to the strong cooling of the polar region throughout the winter. The Arctic ice sheet does not extend far to the south in October. From Kvingedal (2004), it is known that the ice edge normally reaches its southernmost boundary in the beginning of April. The corresponding minimum of ice extent occurs in September. Thus, the mid-level temperatures in October are not especially low, and there will not be as much low-level baroclinicity (and reverse shear in northerly flow) as in March, when the temperatures at mid-levels are generally much lower. This can be seen from the temporal distribution of the low stability-constraint (figure 17). The temperature stays cold throughout March in the Norwegian Sea. In the Sea of Okhotsk, the spring warming takes place earlier, and stability is restored.

The similarities between figures 15 and 17 imply that the two constraints are correlated. In 29 % of all the individual cases inside the NS region over the 40 seasons with reverse-shear conditions, there is also low stability. Conversely, when the stability is low, there is reverse shear 40 % of the time. The corresponding percentages for the Sea of Okhotsk are 8 and 25. In other words, the two conditions are somewhat correlated, especially in the NS region. Again, this is because the passage of extratropical cyclones often leads to both conditions at the same time, due to the proximity of the ice and the northerly winds in reverse shear following the storms. This is probably the main reason for the relatively high frequency of polar low potential in that area.

5.3 Interannual variability

The average percentage of grid points with polar low potential in each region is displayed in figure 18. The standard deviances amount to 3.5 % for NS and 0.9 % for SO. In other words, there is a rather large variability from year to year. In figure 19, the mean yearly NDJFM NAO index is shown. The link to the NAO is clear, but again not one-to-one. In 1968-69 and 1995-96, little polar low potential was recorded in the Norwegian Sea, and these years were also deeply in the negative NAO terrain. On the other hand, 1971-72 also had little potential, but the NAO was positive. Using yearly means is a crude approach, and it must also be remembered that the NAO can not explain everything. However, the connection between the NAO and reverse-shear conditions should be explored further in the future.

6 Conclusions and future directions

Situations during a 40-year period that were characterized by reverse thermal shear and low static stability in the lower layers of the atmosphere have been identified in the ERA-40 data. Such conditions are known to be favourable for polar low development. By defining certain constraints representing such conditions using standard atmospheric fields, it is possible to identify them in any gridded data set. To define the constraints, their behaviour was visualised at the time and location of known polar low developments. For simplicity, discrete threshold values were used. A possible future refinement of the method would be to use multiple thresholds when defining the criteria. It could also be interesting to include a criterion for low-level baroclinicity, which is also considered important for polar low development (Rasmussen and Turner, 2003). However, in the majority of the situations captured by the constraints, it was seen from satellite images that there were at least indications of polar low development. This suggests that it would be meaningful to look for such conditions when forecasting polar lows. It is also possible to apply the constraints to model simulations of future climate scenarios.

An analysis of the spatial and temporal distribution of these conditions constitute a new climatology of reverse-shear polar lows. Such conditions occur with relatively high frequency (10-15 % of the time) throughout the winter months in the Norwegian Sea, a result which is compatible with earlier climatological studies. Several other local maxima for favourable conditions for polar low development were also found: In the region south of the Denmark Strait (around 10 %), in the Bering Sea and in the Sea of Okhotsk (both around 5 %). Two key regions were defined for the study of the seasonal cycle: a sector of the Norwegian Sea and the Sea of Okhotsk. The polar low season in the former region is longer than in the latter. This is mostly because the air temperature stays low for a longer period in the north-eastern Atlantic. The sea-ice maximum there normally occurs in the beginning of April. Because of that and the high latitudes of the region, the temperatures stay low in the Nordic Seas throughout March. During the cold winter months, storms coming into the region from the southwest in positive phases of the NAO are thus likely to be followed by reverse-shear conditions and weak static stability. Furthermore, it was found that there is a relatively quiet period with regards to polar low activity in the Norwegian and Barents Seas around February. This lapse is followed by a brief but significant active period in mid- to late March. The seasonal cycle of the NAO index is at its most negative in February. In March, on the other hand, the average NAO index is considerably higher, indicating that the synoptic storm tracks are more favourable for polar lows then. The link between the NAO and reverse-shear conditions in the Nordic Seas should be explored further. Overall, the Sea of Okhotsk follows a much more defined seasonal cycle, with the peak of polar low potential occurring in mid-December.

REFERENCES

Bluestein, H. B. 1993. *Synoptic-Dynamic Meteorology in Midlatitudes. Volume II: Observations and Theory of Weather Systems*, Oxford University Press.

Bond, N. A. and Shapiro, M. A. 1991. Polar Lows over the Gulf of Alaska in Conditions of Reverse Shear. *Mon. Wea. Rev.* **119**, 551–572.

Claud, C., Heinemann, G., Raustein, E. and McMurdie, L. 2004. Polar low le cygne: Satellite observations and numerical simulations. *Quart. J. R. Meteorol. Soc.* **130**, 1075–1102.

Duncan, C. N. 1977. A numerical investigation of polar lows. *Quart. J. R. Meteorol. Soc.* **103**, 255–267.

Duncan, C. N. 1978. Baroclinic instability in a reversed shear flow. *Meteorological Magazine* **107**, 17–23.

Fu, G., Niino, H., Kimura, R. and Kato, T. 2004. A polar low over the Japan Sea on 21 january 1997. part I: Observational analysis. *Mon. Wea. Rev.* **132**, 1537–1551.

Grønås, S., Foss, A. and Lystad, M. 1987. Numerical simulations of polar lows in the Norwegian Sea. *Tellus* **39A**, 334–353.

Grønås, S. and Kvamstø, N. G. 1995. Numerical simulations of the synoptic conditions and development of arctic outbreak polar lows. *Tellus* **47A**, 797–814.

Harold, J. M., Bigg, G. R. and Turner, J. 1999. Mesocyclone activity over the Northeast Atlantic. part 2: An investigation of causal mechanisms. *International journal of climatology* **19(12)**, 1283–1299.

Holton, J. R. 2004. *An Introduction to Dynamic Meteorology*, Elsevier Academic Press.

Kvingedal, B. 2004. Sea ice extent and variability in the nordic seas, 1967-2002, *AGU Monograph*, 200–210.

Mailhot, J., Hanley, D., Bilodeau, B. and Hertzman, O. 1996. A numerical case study of a polar low in the Labrador Sea. *Tellus* **48A**, 383–402.

Montgomery, M. T. and Farrell, B. F. 1992. Polar low dynamics. *J. Atmos. Sci.* **49**, 2484–2505.

Nordeng, T. E. and Rasmussen, E. A. 1992. A most beautiful polar low - a case study of a polar low development in the Bear Island region. *Tellus* **44A**, 81–99.

Orvik, K. A. and Niiler, P. 2002. Major pathways of Atlantic water in the northern North Atlantic and Nordic Seas toward Arctic. *Geophys. Res. Lett.* **29(19)**, 1896–1899.

Rasmussen, E. A., Pedersen, T. S., Pedersen, L. T. and Turner, J. 1992. Polar lows and arctic instability lows in the Bear Island region. *Tellus* **44A**, 133–154.

Rasmussen, E. A. and Turner, J. 2003. *Polar lows*, Cambridge University Press.

Reed, R. J. and Duncan, C. N. 1987. Baroclinic instability as a mechanism for the serial development of polar lows: a case study. *Tellus* **39A**, 376–385.

Rogers, J. C. 1997. North Atlantic storm track variability and its association to the North Atlantic Oscillation and climate variability of Northern Europe. *J. Clim.* **10(7)**, 1635–1647.

Wilhelmsen, K. 1985. Climatological study of gale-producing polar lows near Norway. *Tellus* **37A**, 451–459.

Wu, B., Wang, J. and Walsh, J. 2004. Possible Feedback of Winter Sea Ice in the Greenland and Barents Seas on the Local Atmosphere. *Mon. Wea. Rev.* **132**, 1868–1876.

Yanase, W., Niino, H. and Saito, K. 2002. High-resolution numerical simulation of a polar low. *Geophys. Res. Lett.* **29(14)**, 1658–1661.

Figure Captions

Figure 1: A satellite image taken of 'le Cygne', taken at 1341 UTC 14 October 1993. Adapted from Claud et al. (2004). Scandinavia is seen in the middle and to the right.

Figure 2: A map of the parameters at 1200 UTC 14 October 1993. Inside the solid contour lines there is reverse shear, i.e. the angle between the 925-700 hPa thermal wind and the wind at the 850-hPa (black) and the 775-hPa (light grey) levels is between 135° and 225°. Inside the dashed contour there is low static stability, i.e. the normalized radius of deformation R_N is less than 25. The regions where both criteria are satified have been filled with dark grey. Iceland is glimpsed on the left, Svalbard in the upper right corner and Scandinavia on the right.

Figure 3: An image of the polar low in Mailhot et al. (1996), taken at 1509 UTC 11 January 1989. Image taken from the Dundee Satellite Receiving Station. Greenland occupies the upper right quarter.

Figure 4: As figure 2, but now at 1200 UTC 12 January 1989. Greenland is seen in the upper right corner and the entrance to the Hudson Strait can be glimpsed on the left.

Figure 5: A reproduction of figure 8a in Fu et al. (2004). This is the Japan Sea with Hokkaido island in the upper right corner.

Figure 6: As figure 2, but now at 1800 UTC 21 January 1997. The area is similar to the one in figure 5.

Figure 7: A satellite image taken on 27 February 1987. The image was taken from http://meted.ucar.edu/norlat/snow/polarlows/. Nothern Scnadinavia is seen in the lower right quarter and Svalbard is glimpsed in the upper left corner.

Figure 8: As figure 2, but now at 0000 UTC 27 February 1987. Northern Scandinavia is at the bottom and Svalbard is barely glimpsed in the upper left corner.

Figure 9: A satellite image taken at 0406 UTC 15 December 1982, and found at the Dundee Satellite Receiving Station. Scandinavia is onthe right, Iceland in the lower left corner, Svalbard in the middle at the top and Greenland in the upper left corner.

Figure 10: As figure 2, but now at 0600 UTC 15 December 1982. The area is similar to the one in figure 9.

Figure 11: The mean percentage of the time during NDJFM 1960-61 to 1999-2000 for each grid point with reverse thermal shear and low static stability according to our constraints.

Figure 12: As in figure 11, but now with the reverse-shear constraint only.

Figure 13: As in figure 11, but now with the low stability constraint only.

Figure 14: The temporal distribution of the number of cases with reverse thermal shear and low static stability in two regions: NS (solid lines) and SO (dashed lines). The values are 40-year averages of daily means of the percentage of the grid points in each region for which the criteria are satisfied for each date from 1 October to 30 April. Quadratic polynomial trends are displayed with thick, black lines and daily means averages with thin, grey lines.

Figure 15: As in figure 14, but now with the reverse-shear constraint only.

Figure 16: The mean monthly NAO index from May 1960 to April 2000. The numbers were obtained from the Climate Prediction Center at http://www.cpc.ncep.noaa.gov.

Figure 17: As in figure 14, but now with the low stability constraint only.

Figure 18: The interannual variability of occurrences of polar low potential for NS (solid line) and SO (dashed line). The values are the average percentage of grid points in each region with reverse shear and weak static stability for each NDJFM season from 1960-61 to 1999-2000.

Figure 19: The yearly mean NDJFM NAO index. The numbers were obtained from the Climate Prediction Center at http://www.cpc.ncep.noaa.gov.

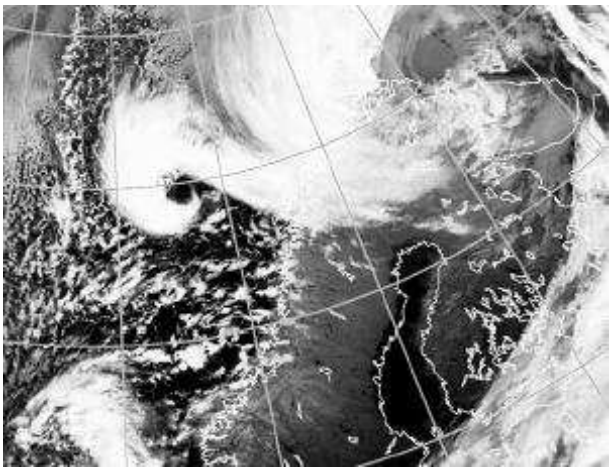

Figure 1. A satellite image taken of 'le Cygne', taken at 1341 UTC 14 October 1993. Adapted from Claud et al. (2004). Scandinavia is seen in the middle and to the right.

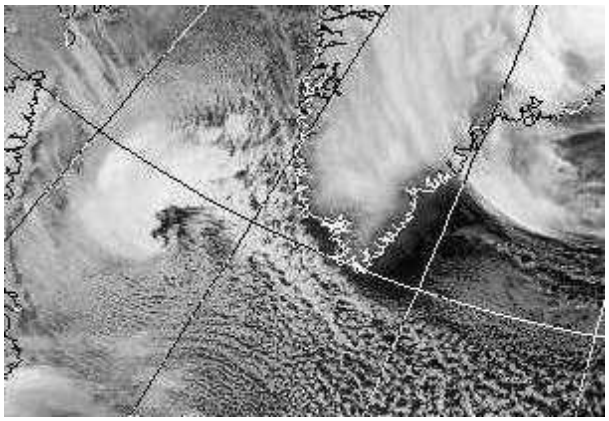

Figure 3. An image of the polar low in Mailhot et al. (1996), taken at 1509 UTC 11 January 1989. Image taken from the Dundee Satellite Receiving Station. Greenland occupies the upper right quarter.

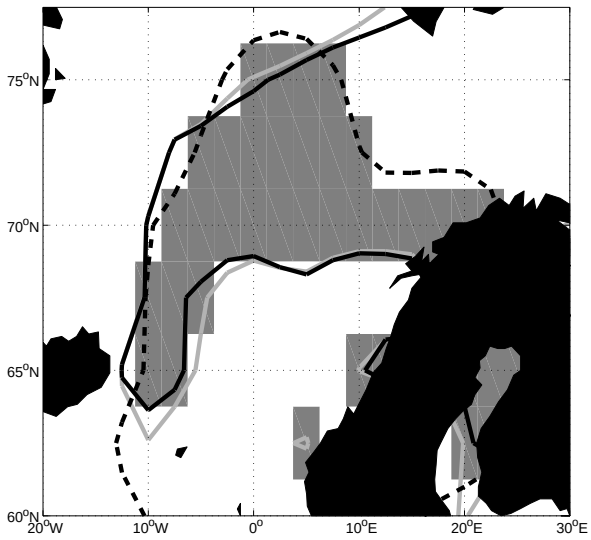

Figure 2. A map of the parameters at 1200 UTC 14 October 1993. Inside the solid contour lines there is reverse shear, i.e. the angle between the 925-700 hPa thermal wind and the wind at the 850-hPa (black) and the 775-hPa (light grey) levels is between 135° and 225°. Inside the dashed contour there is low static stability, i.e. the normalized radius of deformation R_N is less than 25. The regions where both criteria are satified have been filled with dark grey. Iceland is glimpsed on the left, Svalbard in the upper right corner and Scandinavia on the right.

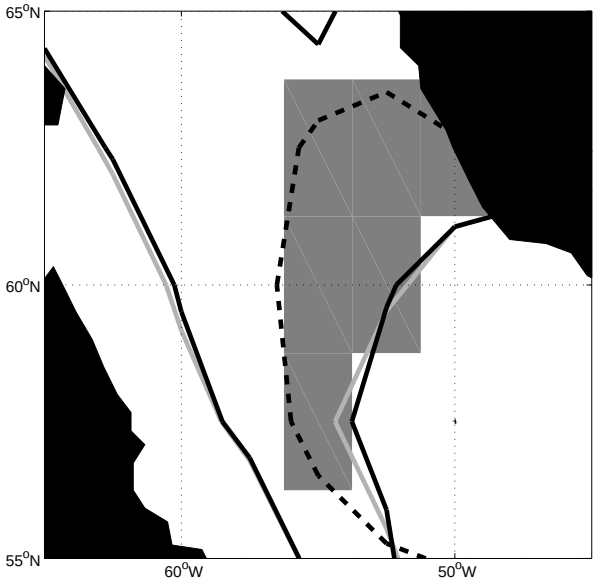

Figure 4. As figure 2, but now at 1200 UTC 12 January 1989. Greenland is seen in the upper right corner and the entrance to the Hudson Strait can be glimpsed on the left.

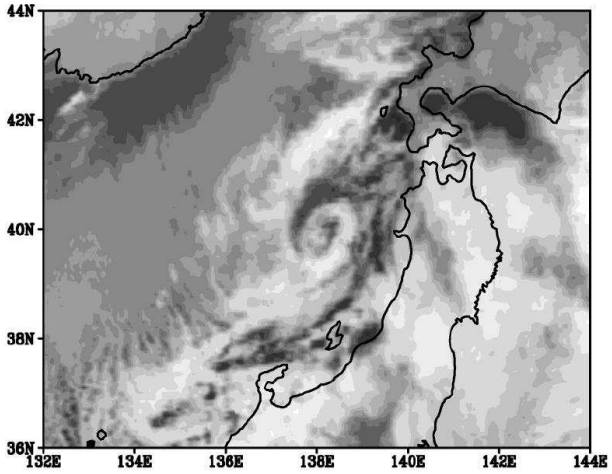

Figure 5. A reproduction of figure 8a in Fu et al. (2004). This is the Japan Sea with Hokkaido island in the upper right corner.

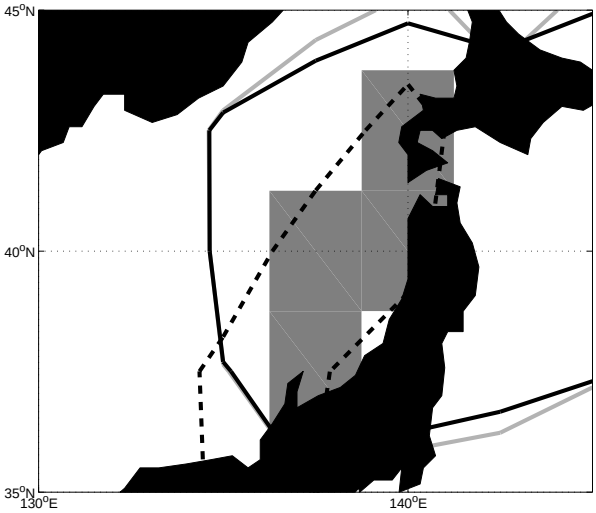

Figure 6. As figure 2, but now at 1800 UTC 21 January 1997. The area is similar to the one in figure 5.

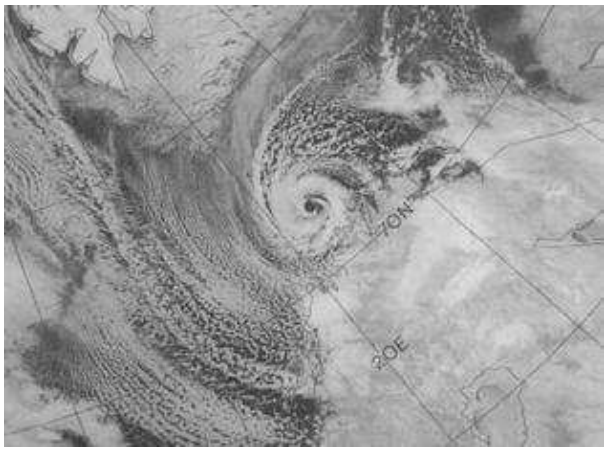

Figure 7. A satellite image taken on 27 February 1987. The image was taken from http://meted.ucar.edu/norlat/snow/polarlows/. Nothern Scnadinavia is seen in the lower right quarter and Svalbard is glimpsed in the upper left corner.

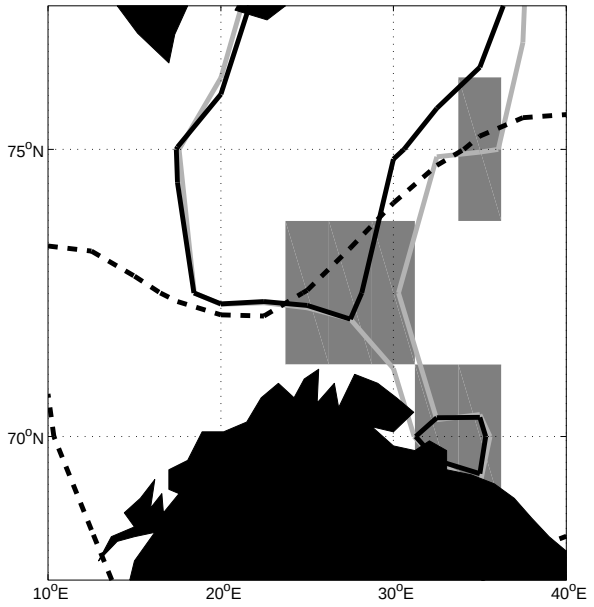

Figure 8. As figure 2, but now at 0000 UTC 27 February 1987. Northern Scandinavia is at the bottom and Svalbard is barely glimpsed in the upper left corner.

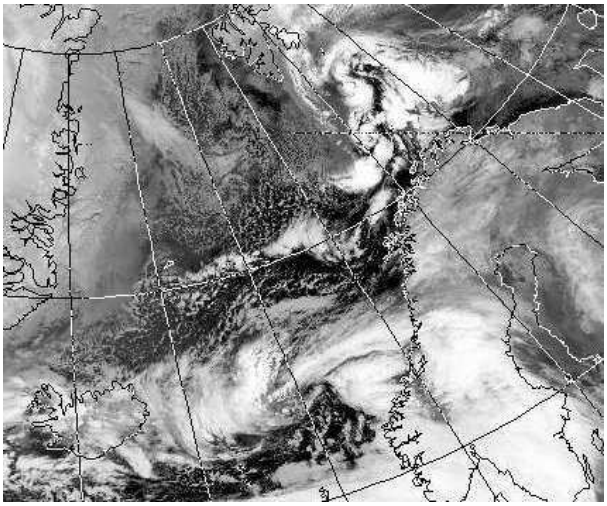

Figure 9. A satellite image taken at 0406 UTC 15 December 1982, and found at the Dundee Satellite Receiving Station. Scandinavia is onthe right, Iceland in the lower left corner, Svalbard in the middle at the top and Greenland in the upper left corner.

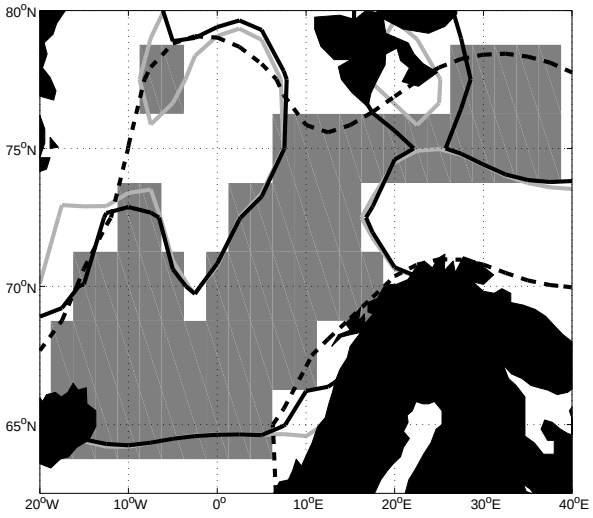

Figure 10. As figure 2, but now at 0600 UTC 15 December 1982. The area is similar to the one in figure 9.

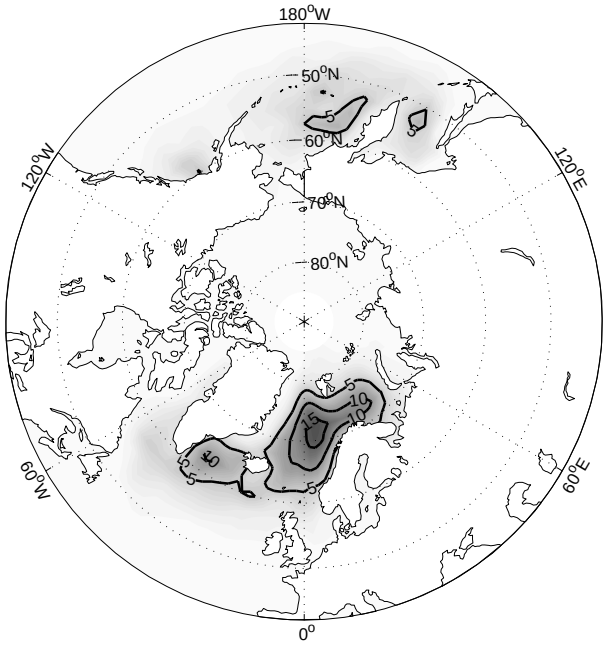

Figure 11. The mean percentage of the time during NDJFM 1960-61 to 1999-2000 for each grid point with reverse thermal shear and low static stability according to our constraints.

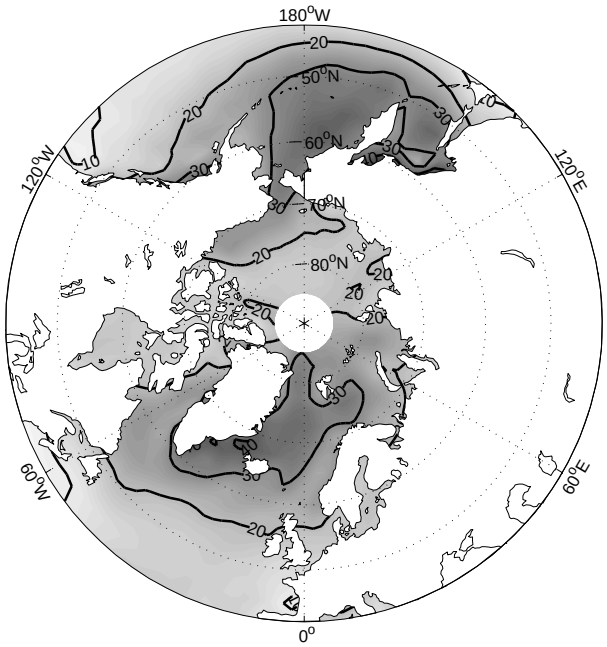

Figure 12. As in figure 11, but now with the reverse-shear constraint only.

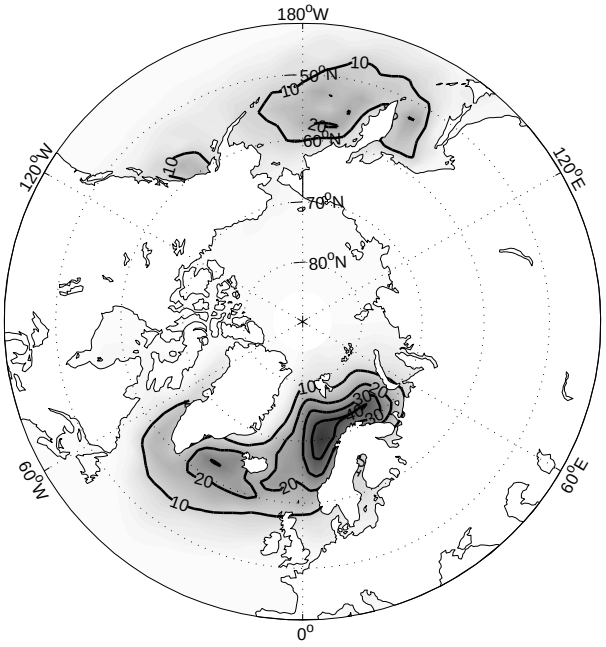

Figure 13. As in figure 11, but now with the low stability constraint only.

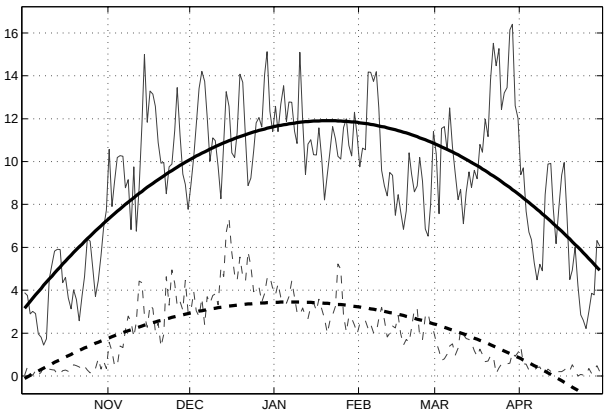

Figure 14. The temporal distribution of the number of cases with reverse thermal shear and low static stability in two regions: NS (solid lines) and SO (dashed lines). The values are 40-year averages of daily means of the percentage of the grid points in each region for which the criteria are satisfied for each date from 1 October to 30 April. Quadratic polynomial trends are displayed with thick, black lines and daily means averages with thin, grey lines.

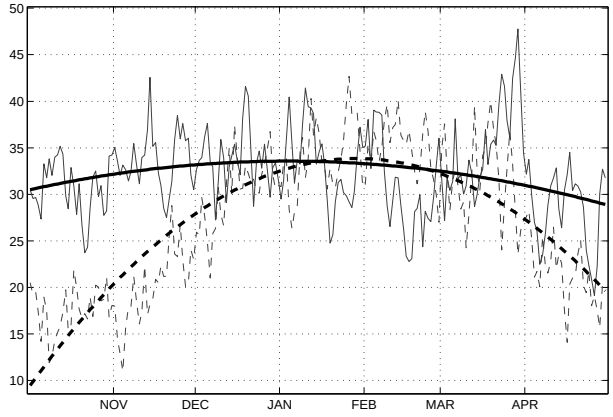

Figure 15. As in figure 14, but now with the reverse-shear constraint only.

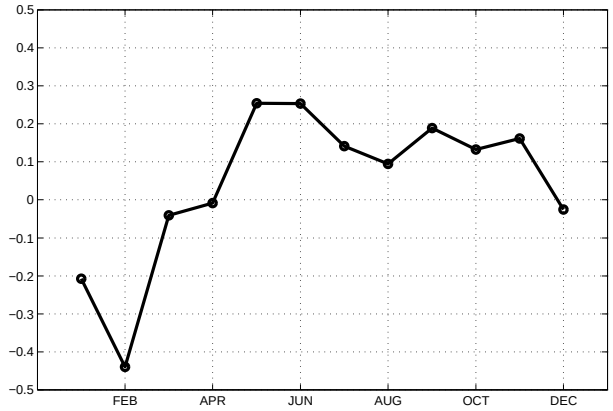

Figure 16. The mean monthly NAO index from May 1960 to April 2000. The numbers were obtained from the Climate Prediction Center at http://www.cpc.ncep.noaa.gov.

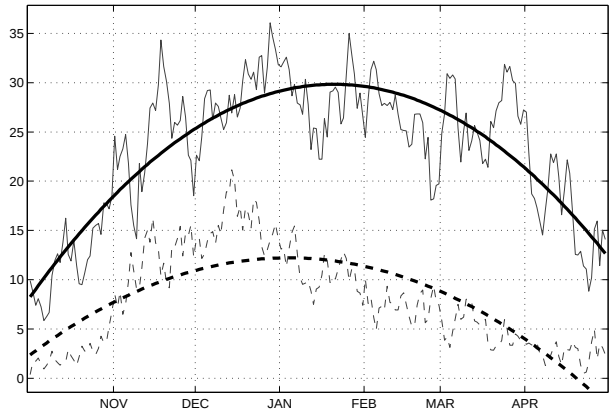

Figure 17. As in figure 14, but now with the low stability constraint only.

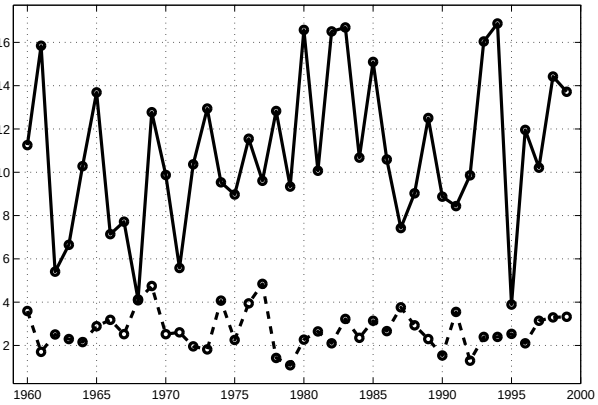

Figure 18. The interannual variability of occurrences of polar low potential for NS (solid line) and SO (dashed line). The values are the average percentage of grid points in each region with reverse shear and weak static stability for each NDJFM season from 1960-61 to 1999-2000.

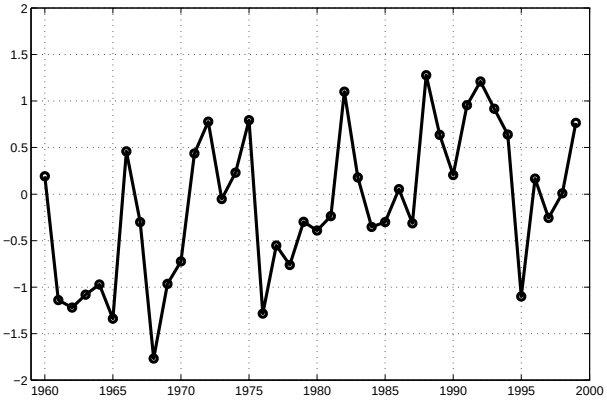

Figure 19. The yearly mean NDJFM NAO index. The numbers were obtained from the Climate Prediction Center at http://www.cpc.ncep.noaa.gov.